point disparities, unless it is assumed that there is an anisotropy in the spatial interactions between disparity processes at a subsequent stage[10].

The experimental findings reported here indicate that the ability to match and discriminate three-dimensional curved surfaces is precise and consistent with the idea of using the differences in curvature of local line elements to represent three-dimensional surfaces. The curvature differences involved are very small, but Watt and Andrews have shown that performance in the discrimination of simple curved lines is indeed at a hyperacuity level[12]. In terms of the underlying physiological mechanisms, Dobbins *et al.*[13] and Orban *et al.*[14] have both shown that end-stopped complex cells in monkey visual cortex are selective for the curvature of line stimuli. A representation of the local curvature properties of a surface by itself, which curvature disparity provides, necessarily excludes information about disparity differences and gradients to which we also need access. Consequently, we are not proposing that second derivative descriptions are the only determinants of our perception of three-dimensional surfaces[15–17], but our experimental evidence suggests that mechanisms have evolved to exploit the fact that curvature disparity (and its equivalent in the optic flow domain[6,18]), remain roughly constant with viewing distance and therefore provide direct information about the local curvature of surfaces in the surrounding world. □

Received 27 September 1988; accepted 30 March 1989.

1. Wheatstone, C. *Proc. R. Soc.* **128,** 371–394 (1838).
2. Julesz, B. *Foundations of Cyclopean Perception* (University of Chicago Press, Chicago, 1971).
3. Ogle, K. N. *Researches in Binocular Vision* (Saunders, Philadelphia, 1950).
4. Mayhew, J. E. W. & Longuet-Higgins, H. C. *Nature* **297,** 376–379 (1982).
5. Gillam, B. & Lawergren, B. *Percept. Psychophys.* **24,** 121–130 (1983).
6. Rogers, B. J. *Nature* **333,** 16–17 (1988).
7. Cagenello, R. & Rogers, B. J. *Invest. Ophthalmol. Vis. Sci.* **29,** 399 (1988).
8. Rogers, B. J. *Invest. Ophthalmol. Vis. Sci.* **27,** 181 (1986).
9. Koenderink, J. J. *Vision Res.* **26,** 161–179 (1986).
10. Rogers, B. J. & Graham, M. E. *Science* **221,** 1409–1411 (1983).
11. Cagenello, R. B. & Rogers, B. J. *Perception* **17,** 366, Abstract (1988).
12. Watt, R. J. & Andrews, D. P. *Vision Res.* **22,** 449–460 (1982).
13. Dobbins, A., Zucker, S. & Cynader, M. *Nature* **329,** 438–441 (1987).
14. Orban, G., Versavel, M. & Lagae, L. *Soc. Neurosci. Abstr.* **13,** 1451 (1987).
15. von der Heydt, R., Adorjani, C. & Hanny, P. *Experientia* **33,** 786 (1977).
16. Blakemore, C., Fiorentini, A. & Maffei, L. *J. Physiol.* **226,** 725–749 (1972).
17. Blakemore, C. *Vision Res.* **10,** 1181–1199 (1970).
18. Rogers, B. J. & Graham, M. E. *Perception* **8,** 125–134 (1979).
19. Tyler, C. W. *Science* **181,** 276–278 (1973).
20. Burt, P. & Julesz, B. *Perception* **9,** 671–682 (1980).

A retina with at least ten spectral types of photoreceptors in a mantis shrimp

Thomas W. Cronin* & N. Justin Marshall†

* Department of Biological Sciences, University of Maryland, Baltimore County, Catonsville, Maryland 21228, USA
† School of Biological Sciences, University of Sussex, Falmer, Brighton BN1 9QG, UK

STOMATOPOD crustaceans, commonly named mantis shrimps, have compound eyes of unique design. A central band composed of six parallel rows of ommatidia separates two peripheral ommatidial groups, and all three regions view the same area of visual space[1–3]. In the central bands of members of the stomatopod superfamily Gonodactyloidea, four of the ommatidial rows are built of tiers of photoreceptors; in two of these rows, the photoreceptors themselves contain coloured filters[4]. Such a design could in principle produce many spectral classes of photoreceptors using only a single visual pigment[4,5]. We measured the absorption spectra of the coloured filters and the visual pigments in frozen sections of retinae of a typical species, *Pseudosquilla ciliata*, using end-on microspectrophotometry. The retina contains not one, but as many as ten visual pigments, each in a distinct photoreceptor class, having maximum absorbances at wavelengths from 400 to 539 nm. Because of the unique anatomy of stomatopod eyes, ten or more spectral types of photoreceptors exist in this species.

The retina of *P. ciliata* has 11 classes of photoreceptors, or rhabdoms, below the level of the distal eighth retinular cell: the single rhabdoms of the peripheral retina and rows 5 and 6 of the central band, plus the two tiers of the main rhabdoms of rows 1 to 4 of the central band (Fig. 1). Rows 2 and 3 of the central band each contain two intrarhabdomal filters. Their absorption spectra resemble those of carotenoid pigments, and have rapidly falling absorbances on the long-wavelength limb (Fig. 2). In both rows, the distal filter (F1) has a 50% transmission point at shorter wavelengths than that of the proximal filter (F2). The filters thus operate in series, permitting light of a greater spectral range to penetrate the distal rhabdom than the proximal rhabdom. Maximum optical densities of these filters were relatively high, ranging from 1.35 to 11.1 density units.

Crustaceans have bistable visual pigments; the photopigment, usually termed rhodopsin, is interconvertible with a thermally stable metarhodopsin[6]. Because only the rhodopsin form takes part in photoreception, however, we needed to know only its absorption spectrum. We therefore maximized rhodopsin content in the retina by dark-adapting experimental animals at least overnight, and commonly for several days (overnight dark adaptation normally produces ~100% rhodopsin in all photoreceptors of crustaceans[7–9]). The rhodopsin absorption spectrum was then obtained by subtracting the absorption spectrum of the fully photobleached photoreceptor from the spectrum of the same receptor when dark-adapted.

Rhodopsin did, in fact, initially predominate in the retinae. Exposure to bright red light produced a rise in absorption, and a shift of the maximum to shorter wavelengths, in photoreceptors of the peripheral retina and rows 2, 5 and 6 of the central band. Such changes are typical of crustacean rhodopsins having maxima near 500 nm, and reveal the net conversion of rhodopsin to metarhodopsin[6–10]. Additionally, most photobleach spectra closely resembled template rhodopsin spectra (Fig. 2); it is not possible to fit mixtures of photopigments to rhodopsin templates[8,10]. The close fits (with two exceptions; see below) also show that the phototreatment produced no stable products having spectra that overlapped the rhodopsin spectrum[10]. Photobleaching produced typical density losses of 0.003–0.008 μm^{-1}, similar to average axial densities of rhodopsin in other crustacean rhabdoms[9,11,12].

No evidence was found for any pigment photobleaching in the spectral range from 400–700 nm in any rhabdomeres of 8th retinular cells, and it is possible that these contain a visual pigment absorbing maximally at shorter wavelenths. All main rhabdoms, built from retinular cells 1–7, contained photopigments absorbing in this region. The photopigment of rows 5 and 6 of the central band absorbed maximally at 510 nm (Fig. 2). Rhabdoms of the peripheral retina had a second visual pigment absorbing maximally at 498 nm. Moreover, each tier of ommatidial rows 1–4 in the central band contained a different visual pigment. In every case, the rhodopsin of the distal tier had a shorter λ_{max} than that of the proximal tier, usually differing by about 25 nm. This arrangement allows the rhodopsin of the distal tier to act as a long-pass filter. Light entering the proximal rhabdomal region would then be limited to wavelenths absorbed mainly by the long-wavelength limb of the rhodopsin residing there, sharpening the spectral sensitivity.

Overall, the close correspondences of the averaged photobleach data to the rhodopsin template curves indicate that each region possesses only a single photopigment which is actually a true rhodopsin with a retinoid chromophore. The poorest fits occur in row 3, where rhabdoms are particularly difficult to sample because they are densely coated with granules of screening pigment and rarely offer a clear path for spectral scanning

(Fig. 1). The photobleach difference spectrum of the distal tier of row 1 also differs from the template; it drops more rapidly from its peak and has negative values between 450 and 600 nm. This indicates that the photobleaching exposure produced persistent, relatively stable photoproducts absorbing at longer wavelengths than the rhodopsin. A suggestion of the same effect is apparent in the distal tier of row 4.

In determining the dark-adapted spectral sensitivity functions for the sampled retinal regions, it was assumed that absorption by the dioptric apparatus (cornea and crystalline cone) and the short rhabdomere of the 8th retinular cell was negligible, and that each main rhabdom or tier contained no stable photoproducts. When the main rhabdom was untiered, spectral sensitivity was taken to be proportional to the absorptance (fraction of light absorbed) of the visual pigment. This was computed using the best-fit rhodopsin template spectra, the rhabdomal length measured in frozen material sectioned axially, and an estimate of the axial density. As the beam of the microspectrophotometer passed along the axis of the rhabdom, traversing numerous microvillar layers, photopigment axial densities could be estimated directly from the photobleach data. The value used in the computations was that of the largest photobleaches, 0.008 density units per micrometre.

In the tiered rows, determination of spectral sensitivity was complicated by the fact that the light entering each tier was modified by absorption in any overlying photopigments and filters. In rows without filters, the spectral sensitivity of the distal tier was again proportional to the rhodopsin absorptance, and that of the proximal tier was computed by taking the product of the transmittance spectrum of the distal tier and the absorptance spectrum of the proximal tier. Rhabdoms with filters had several successive light-modifying levels, so the sensitivity spectrum of each tier was obtained by iterating this procedure.

The typical, untiered rhabdoms have broad, flat-topped sensitivity functions, ideal for photon capture and for the analysis of polarized light (Fig. 3). These are the tasks for which these retinal regions seem to be anatomically designed[4]. In rows 1–4, however, each rhabdom includes a pair of photoreceptor classes with narrow spectral sensitivities. Except for row 3, these pairs are separated by about 50 nm, which could permit excellent spectral discrimination in the wavelength range between their peaks. Together, the four rows cover the spectrum from 400–630 nm (Fig. 3).

P. ciliata thus possesses a retina with many spectral classes of photoreceptors, produced by a variety of visual pigments which, in combination with stacked photostable filters, modify and spectrally sharpen the light passing through successive retinal tiers. We have examined the retina of another gonodactyloid, *Gonodactylus oerstedii*, in less detail, and find that it is organized much like that of *P. ciliata*. One difference, however, is that in *G. oerstedii*, the spectral separations of both the filters and photopigments of row 3 of the central band are greater than in *P. ciliata*. This combination produces a pair of sensitivity functions peaking near 560 and 620 nm.

The diversities of both the visual pigments and the spectral classes in this stomatopod retina are the greatest known in any visual system. Among vertebrates, up to five spectral types of photoreceptors have been found in some fish retinae[13,14]. The cone photoreceptors of birds and reptiles sometimes contain three or four cone visual pigments together with photostable oil droplet filters, for a total of at least four spectral classes of photoreceptors[15–17]. Main rhabdoms of crustaceans usually have only a single rhodopsin, absorbing maximally between 450 and 550 nm[8,9]; another type absorbing at shorter wavelengths may occur in the rhabdomere of the 8th retinular cell[18]. Of other invertebrates, flies possess the greatest visual pigment diversity previously known, with at least five distinct visual pigment classes (summarized in ref. 19). Some butterflies have

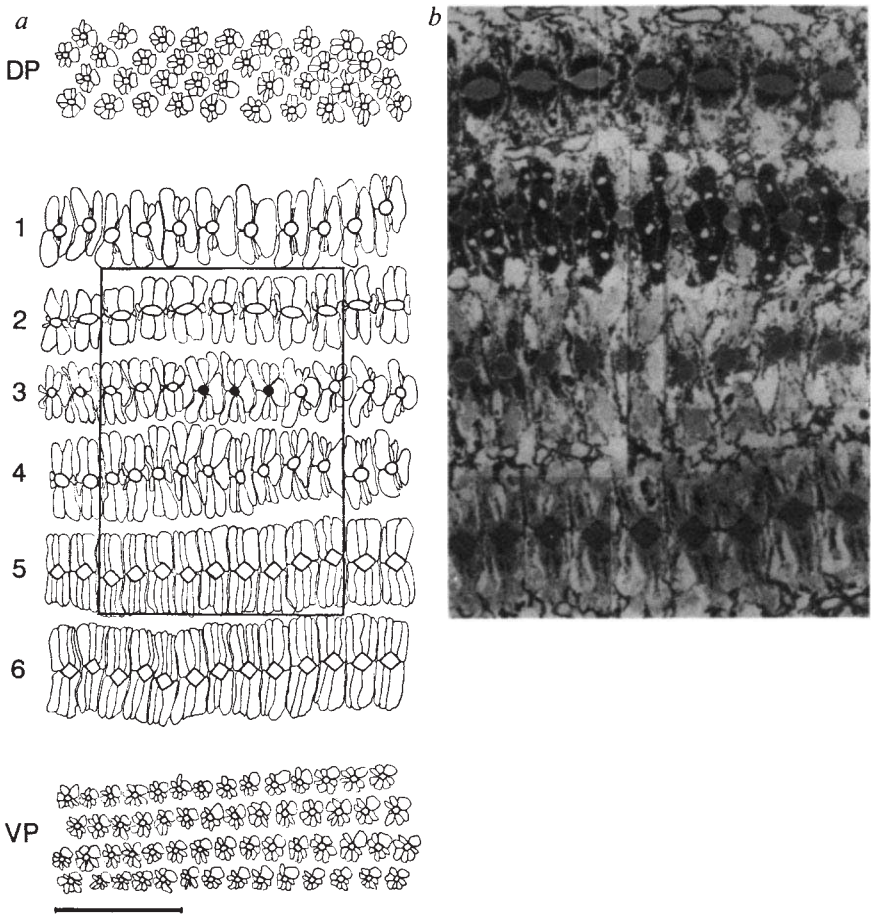

FIG. 1 *a*, Retina of *P. ciliata*. The rhabdoms and retinular cells have been traced from photographs of a fixed and toluidine blue-stained section. The cryosections used for microspectrophotometry were similar but less well organized. The peripheral ommatidia and rows of the central band are indicated. DP, dorsal peripheral retina; VP, ventral peripheral retina; 1–6, rows of the central band. The section was made near the level where the proximal and distal tiers of central band rows 1–4 meet. The dark centres in three ommatidia of row 3 indicate the presence of proximal filters (F2). To the right of the filters, the rhabdoms of row 3 are surrounded by three pigmented cells, which are the retinular cells that build rhabdoms in the distal tier, whereas to the left each rhabdom is surrounded by the four retinular cells that build the proximal tier. Note that the ommatidia of central band rows 1–4 have circular rhabdoms of varying morphology, whereas rows 5 and 6 have similar, square rhabdomal cross-sections. The ommatidia of the dorsal and ventral regions, in the peripheral retina, are all similar and are packed into a typical crustacean hexagonal lattice. Scale bar, 100 μm. *b*, A section of the photographic montage from which the tracing on the right was made, showing ommatidia of rows 2–5 of the central band. Its location on the tracing is indicated by the rectangle.

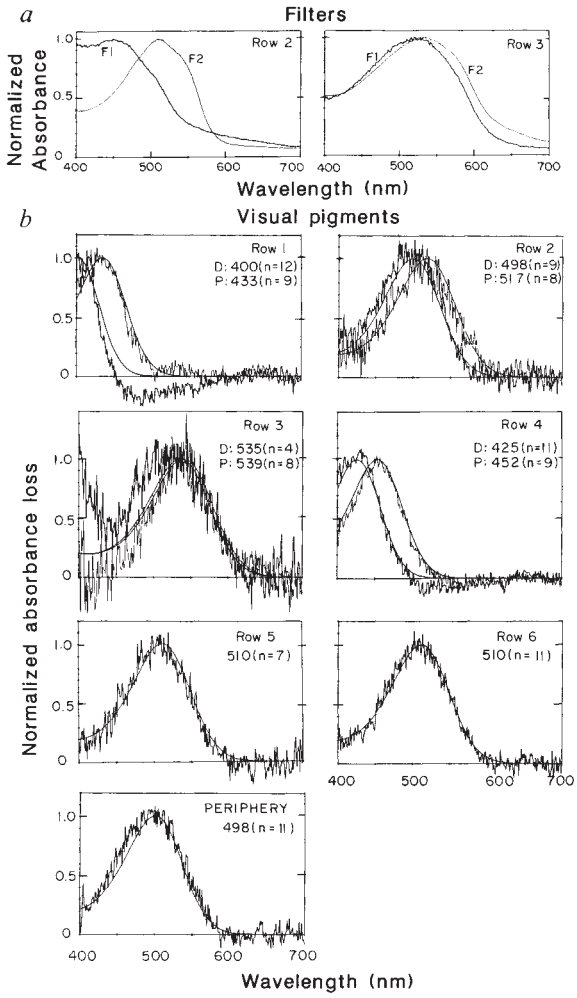

FIG. 2 *a*, Absorption spectra of intrarhabdomal filters of *P. ciliata*. Each spectrum has been normalized to its peak. F1, distal filter; F2, proximal filter. Peak absorbances of the entire filters *in vivo*: row 2 (F1), 1.35; row 2 (F2), 6.1; row 3 (F1), 4.9; row 3 (F2), 11.1. *b*, Normalized, average difference spectra for photobleaching of visual pigments in all retinal regions (jagged traces), and best-fit template curves (smooth traces). The best-fit curves are computed from an 8th-order polynomial derived from vertebrate cone visual pigment data by G. D. Bernard[25]. Any drifts in the photobleach curves have been removed by setting the average absorbance change from 651–700 nm equal to 0. The number of individual photobleaches included in the average is provided on each panel, as is the λ_{max} of the best-fit rhodopsin template curve (D, distal rhabdomal tier; P, proximal rhabdomal tier).

METHODS. Eyes of fully dark-adapted animals were removed in dim red light and either fixed overnight in 0.5% glutaraldehyde in phosphate buffer (pH 7.4) and subsequently cryoprotected in a solution of 30% sucrose in the same buffer, or quick-frozen with Freon spray immediately after removal. Whole frozen eyes were mounted in a cryostat, and 8-μm sections were cut under dim red light in the plane transverse to the rhabdomal axes of ommatidia of the central band. Sections were placed in a drop of buffer inside a ring of silicone grease between 2 coverslips and mounted in the microspectrophotometer. The instrument used was of single-beam design; scans were made from 400–700 nm using a circular 1.5-μm spot of linearly polarized light (see also refs 8 and 9). In cases where the peak optical density of an intrarhabdomal filter was too great for precise determination ($OD_{max} > 2.5$), scans were taken both of filters occupying the full 8-μm thickness of the section and of identical filters sectioned only partially. Axial density per μm was determined by scaling the spectra of the thinner sections to overlie the spectral regions that could be measured from the full sections, and the total density was obtained by taking the product of the density per μm and the lengths of the filters measured in longitudinal frozen sections. Absorption spectra of the rhodopsins were obtained by placing the 1.5-μm beam centrally in rhabdoms having unobstructed end-on orientation within the section. The spectrum of the dark-adapted photoreceptor was first measured, the visual pigment was then fully photobleached with a 2–5 min exposure to high-intensity white light. The receptor is considered photobleached when the spectrum could no longer be altered by further exposure to bright white light. In aldehyde fixative, crustacean photopigments photobleach readily[7–9]; those of *P. ciliata* were equally susceptible to photobleaching in frozen sections from unfixed eyes. A second spectral scan was taken and the difference between the two scans represented the absorption spectrum of the photopigment. Data from photobleaches of 4–12 rhabdoms of each class were averaged, and each visual pigment was identified by subjecting the averaged data to a least-squares analysis of fit to an idealized visual pigment absorption spectrum[9].

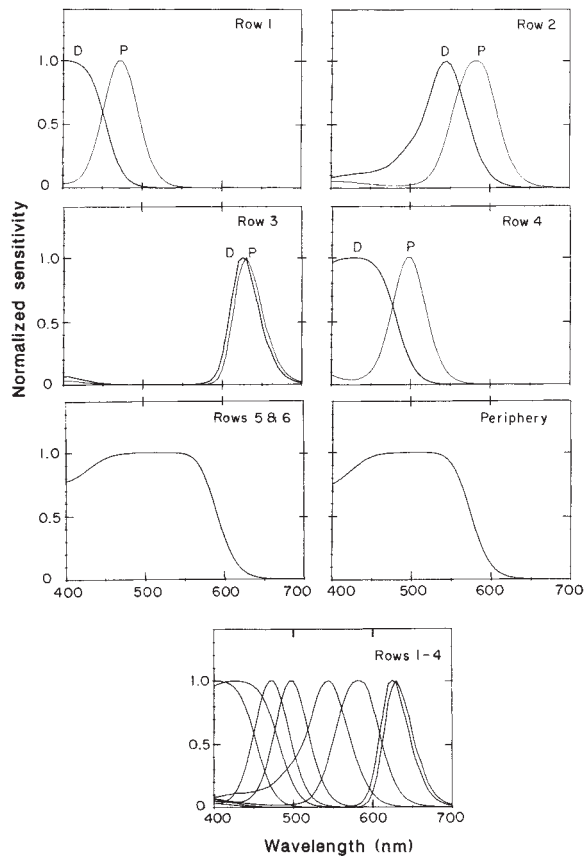

FIG. 3 Normalized sensitivity spectra for all retinal regions, computed as described in the text. Computations use the filter densities of Fig. 2, an axial density of visual pigment of 0.008 μm^{-1}, and rhabdomal lengths of 150–200 μm for the tiers (rows 1–4), 400 μm for rows 5 and 6 of the central band, and 350 μm for peripheral rhabdoms. The two tiers of ommatidial rows 1–4 of the central band are illustrated in the top four panels (D, distal rhabdomal tier; P, proximal rhabdomal tier), whereas functions for untiered rhabdoms are plotted separately below. The bottom panel includes all sensitivity spectra for the four most dorsal rows of the central band.

pentachromatic vision, produced by an unknown number of visual pigments[20].

What advantages are conferred by the presence of such a variety of photoreceptor spectral classes? As mantis shrimps are diurnally active and live in shallow, clear water[21], they live in a visual environment similar to that of terrestrial animals. Visual pigments characteristically have broad absorption spectra, so that only three or four distinct functional classes can operate in the wavelength band from 400–700 nm[22,23]. By narrowing the spectral acceptance functions of photoreceptors in rows 1–4 of the central band, *P. ciliata* has beaten this theoretical constraint. Its visual system could, in principle, discriminate among spectra that have broadly similar shapes, but differ slightly in detail. Stomatopods are brightly coloured animals. Some of their markings have species-specific colours, but the hues of others vary considerably among individuals[21,24]. Recognition of fine spectral detail may play an important part in intraspecific communication and in the recognition of individuals. □

Received 6 February; accepted 31 March 1989.

1. Horridge, G. A. *Phil. Trans. R. Soc.* **285**, 1–59 (1978).
2. Schiff, H. & Candone, P. *Comp. Biochem. Physiol.* **83A**, 445–455 (1986).
3. Cronin, T. W. *J. crust. Biol.* **6**, 1–23 (1986).
4. Marshall, N. J. *Nature* **333**, 557–560 (1988).
5. Hardie, R. C. *Nature* **333**, 499–500 (1988).
6. Stavenga, D. G. & Schwemer, J. in *Photoreception and Vision in Invertebrates* (ed. Ali, M. A.) 11–61 (Plenum, New York, 1984).
7. Goldsmith, T. H. *Vision Res.* **18**, 463–473 (1978).
8. Cronin, T. W. *J. comp. Physiol.* A**156**, 679–687 (1985).

9. Cronin, T. W. & Forward, R. B., Jr *J. comp. Physiol.* A**162,** 463–478 (1988).
10. Lipetz, L. E. & Cronin, T. W. *Vision Res.* **28,** 1083–1093 (1988).
11. Bruno, M. S., Barnes, S. N. & Goldsmith, T. H. *J. comp. Physiol.* **120,** 123–142 (1977).
12. Hiller-Adams, P., Widder, E. A. & Case, J. F. *J. comp. Physiol.* A**163,** 63–72 (1988).
13. Avery, J. A., Bowmaker, J. K., Djamgoz, M. B. A. & Downing, J. E. G. *J. Physiol., Lond.* **334,** 23P-24P (1983).
14. Hårosi, F. I. & Hashimoto, Y. *Science* **222,** 1021–1023 (1983).
15. Ohtsuka, T. *J. comp. Neurol.* **237,** 145–154 (1985).
16. Ohtsuka, T. *Science* **229,** 874–877 (1985).
17. Jane, S. D. & Bowmaker, J. K. *J. comp. Physiol.* A**162,** 225–235 (1988).
18. Cummins, D. R. & Goldsmith, T. H. *J. comp. Physiol.* **142,** 199–202 (1981).
19. Hardie, R. C. in *Progress in Sensory Physiology* Vol. 5 (ed. Ottoson, D.) 1–79 (Springer, Berlin, 1985).
20. Arikawa, K., Inokuma, K. & Eguchi, E. *Naturwissenschaften* **74,** 297–298 (1987).
21. Caldwell, R. L. & Dingle, H. *Naturwissenschaften* **62,** 214–222 (1975).
22. Barlow, H. B. *Vision Res.* **22,** 635–643 (1982).
23. Bowmaker, J. K. *Trends neurosci.* **6(2),** 41–43 (1983).
24. Dingle, H. *Crustaceana* **7,** 236–240 (1964).
25. Bernard, G. D. *J. opt. Soc. Am.* **A4,** 123 (1987).

ACKNOWLEDGEMENTS. We thank G. D. Bernard, T. H. Goldsmith and M. F. Land for commenting on the manuscript, and G. D. Bernard for use of his rhodopsin template polynomial. This work was supported by the US National Science Foundation and by the UK Science and Engineering Research Council.

Accelerated evolution of a false-truffle from a mushroom ancestor

Thomas D. Bruns*§, Robert Fogel†, Thomas J. White‡ & Jeffrey D. Palmer†

* Department of Botany, University of California, Berkeley, California 94720, USA
† Department of Biology, University of Michigan, Ann Arbor, Michigan 48109-1048, USA
‡ Cetus Corporation, 1400 Fifty-third Street, Emeryville, California 94608, USA

THE false-truffles (Hymenogastrales) are a group of basidiomycetous fungi that produce underground truffle-like basidiocarps. They are generally believed to be independently derived from several mushroom lineages[1–4], but extensive morphological divergence often obscures recognition of these phylogenetic connections. Comparisons of mitochondrial DNA now demonstrate a surprisingly close relationship between species of false-truffles in the genus *Rhizopogon* (Hymenogastraceae) and the mushroom genus *Suillus* (Boletaceae). The striking morphological differences separating all *Suillus* species from *Rhizopogon* imply an acceleration in the rate of morphological change relative to molecular change during the evolution of these false-truffles from their mushroom ancestors. This acceleration can best be explained by rapid morphological divergence resulting from selective pressures which may have acted on a small number of developmental genes.

§ To whom correspondence should be addressed.

Two types of molecular evidence demonstrate that *Rhizopogon* is closely related to *Suillus*. First, the structure of the mitochondrial genome of *Rhizopogon subcaerulescens* is identical to that of 14 species of *Suillus* with respect to the order of 15 regions (Fig. 1). The common order of these fragments in *Suillus* and *R. subcaerulescens* is highly significant because mitochondrial gene order is known to be extremely variable among distantly related species of fungi[5–7], and because differences in the order of these 15 regions exist both within the genus *Suillus* and among related genera of the Boletaceae[8]. Second, nucleotide sequences from a portion of the mitochondrial large subunit ribosomal RNA gene from two species *Rhizopogon*, three species of *Suillus* and three species from other genera in the Boletaceae, demonstrate a high level of similarity between *Rhizopogon* and *Suillus* and significant divergence of both of these genera from the other members of Boletaceae sampled (Fig. 2). Cladistic analyses of these sequences demonstrate that *Rhizopogon* and *Suillus* are a monophyletic group that has diverged significantly from the three members of the Boletaceae sampled (Fig. 3).

The extreme morphological divergence between *Rhizopogon* and *Suillus* provides a striking contrast to their molecular similarity. *Suillus* shares many obvious morphological similarities with *Paragyrodon sphaerosporus* such as the presence of tubes, annulate stipes and large pilei. Microscopic features of their basidia and spore attachment are also similar, and the latter species has previously been placed within *Suillus*[9]. *Rhizopogon* differs from both taxa with respect to all of these features and has traditionally been placed in a different family or order[10–12], but molecular criteria (Figs 1 and 2) demonstrate that it is more closely related to *Suillus* than either *Suillus* or *Rhizopogon* is to *P. sphaerosporus*. These results demonstrate an accelerated rate of morphological change relative to molecular change during the evolution of *Rhizopogon*.

This acceleration can be caused by either an increase in the rate of morphological evolution or a decrease in the rate of molecular divergence in *Rhizopogon*, relative to the other taxa studied. The latter explanation would require a major departure from the molecular clock hypothesis, and would not explain the structural similarity of the mitochondrial genomes (Fig. 1). The rate of sequence divergence in *Rhizopogon* would have had to have a fourfold decrease just to set its time of divergence from its closest relatives within *Suillus* to that of its nearest mushroom relative outside the genus (that is, *P. sphaerosporus*), and even this adjustment would be insufficient to match the morphological divergence between *Rhizopogon* and *Suillus* to an outside point of reference. Furthermore, this fourfold rate difference clearly represents an underestimation, because four regions of the gene that align well in comparisons of *Suillus* and *Rhizopogon* were excluded from comparisons with the highly divergent sequences of the other three members of the Boletaceae (Fig. 2). Deviations

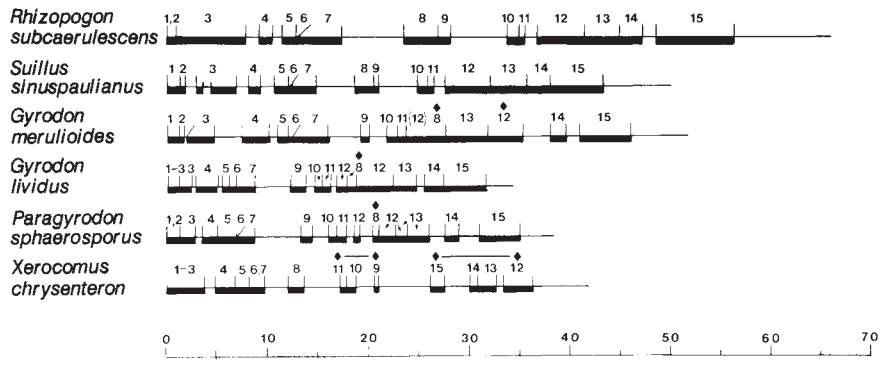

FIG. 1 Fragment order of *R. subcaerulescens* and five taxa from the Boletaceae. The circular mitochondrial genomes of the six taxa are shown linearized in approximate alignment. Regions that hybridize to 14 cloned fragments of *Suillus* mitochondrial DNA (mtDNA) and to portions of the ATPase 9 gene of *Saccharomyces cerevisiae* (region 8) were determined by Southern blot hydridizations. The fragment order shown in *S. sinuspaulianus* is shared by 14 of the 15 species of *Suillus* previously examined[8]. Rearrangements relative to this predominate *Suillus* order were not found in *R. subcaerulescens* but do exist (diamonds) in all other members of the Boletaceae sampled previously[8]. Approximately 75% of the *S. sinuspaulianus* mitochondrial genome and at least eight mitochondrial genes are included in these fragments[8]. MtDNA size varies threefold within *Suillus*[7] and is a poor indicator of phylogenetic affinity[8]. Size scale at the bottom is in kilobase pairs. Light hybridization of clone 12 to a portion of the *G. merulioides* genome is shown with parentheses. The clones, hydridization conditions, and restriction enzymes mapped are described elsewhere[8].